Supplementary Material

June 17, 2024

Contents

1 SHYFEM-Hg user manual

The coupling between the Hg modules for mercury and particles and the SHYFEM model is meant to provide a tool for investigating the biogeochemical dynamics of Hg species in water and sediment, including dynamic exchanges between the two compartments.

SHYFEM (System of HydrodYnamic Finite Element Modules) is a software designed to resolve the hydrodynamic equations in lagoons, coastal seas, estuaries, and lakes. It is provided under the GPL license and can be downloaded with the complete user manual from the official site (https://sites.google.com/site/SHYFEM/). Here, a description of the formulation and usage of the routines for mercury and particles is provided.

1.1 General Description

The mercury model was derived from the WASP Hg module released by the U.S. Environmental Protection Agency (EPA) [1] and modified following [2, 3, 4, 5, 6]. The model (Fig. 1) simulates the evolution of three Hg state variables (Table 1) and includes a module that deals with three types of sediment particles state variables (Table 2) in the water column and in the seabed. The model is composed of 5 subroutines as synthesized in Table 3. The mercury state variables (Hg_i) represent the pool of three main species, namely, oxidized inorganic mercury (Hg^{II}), elemental mercury (Hg^0), and methylmercury ($MeHg$). The sediment state variables (P_i) include different types of inorganic and organic particles: silt, refractory particulate organic matter (POM_{ref}), and labile organic matter (POM_{lab}).

The partitioning of Hg species among particulate and dissolved phases in water and sediment depends on the partition coefficients $K_{D_{Hg_i-P_i}}$, as described by the equations of Table 4. The three Hg species are interconnected through biogeochemical transformations occurring in water ($J^{bgc}_{(Hg_i)_w}$) and sediment ($J^{bgc}_{(Hg_i)_s}$) nodes of the model (Table 5). The transport of particulate Hg^{II} and $MeHg$ (Table 6) is mediated by the deposition and resuspension of the sediment state variables (Silt, POM_R, and POM_L), which in turn are regulated by the bottom shear stress. Dissolved Hg species are instead exchanged through diffusion between pore-water and water (Table 6). Hg^0 is a dissolved gas that is exchanged with the atmosphere (Table 7). All the Hg species are transported with advective fluxes.

To use the mercury and sediment modules, the following flags need to be set in the subroutine `mercury.f`:

```
breact = .true.
what = 'mercury'
```

$\frac{\partial Hg}{\partial t} = Q(Hg_i)_j$		*General Reactor Equations*
$Q(Hg^0)_w = J^{bgc}_{Hg^0_w} - J^{diff}_{Hg^0} + J^{evs}_{Hg^0}$	1	Elemental mercury Hg^0 in water [ng Hg/L]
$Q(Hg^{II})_w = J^{bgc}_{Hg^{II}_w} - J^{diff}_{Hg^{II}} + J^{res}_{Hg^{II}_s} - J^{dep}_{Hg^{II}_w}$	2	Oxidized mercury Hg^{II} in water [ng Hg/L]
$Q(MeHg)_w = J^{bgc}_{MeHg_w} - J^{diff}_{MeHg} + J^{res}_{MeHg_s} - J^{dep}_{MeHg_w}$	3	Methylmercury $MeHg$ in water [ng Hg/L]
$Q(Hg^0)_s = J^{bgc}_{Hg^0_s} + J^{diff}_{Hg^0}$	4	Elemental mercury Hg^0 in sediment [ng Hg/L]
$Q(Hg^{II})_s = J^{bgc}_{Hg^{II}_s} + J^{diff}_{Hg^{II}} - J^{res}_{Hg^{II}_s} + J^{dep}_{Hg^{II}_w}$	5	Oxidized mercury Hg^{II} in sediment [ng Hg/L]
$Q(MeHg)_s = J^{bgc}_{MeHg_s} - J^{diff}_{MeHg} - J^{res}_{MeHg_s} + J^{dep}_{MeHg_w}$	6	Methylmercury $MeHg$ in sediment [ng Hg/L]

Table 1: Mass balances for Hg species in water and sediment

$\frac{\partial S}{\partial t} = Q(P_i)_j$		*General Reactor Equations*
$Q(silt)_w = J^{res}_{silt_s} - J^{dep}_{silt_w}$	7	Silt in water [mg silt/L]
$Q(POM_R)_w = J^{res}_{POM_{R_s}} - J^{dep}_{POM_{R_w}} - J^{deg}_{POM_{R_w}}$	8	Refractory POM in water [mg OM/L]
$Q(POM_L)_w = J^{res}_{POM_{L_s}} - J^{dep}_{POM_{L_w}} + J^{PP}_{POM_{L_w}} - J^{deg}_{POM_{L_w}}$	9	Labile POM in water [mg OM/L]
$Q(silt)_s = -J^{res}_{silt_s} + J^{dep}_{silt_w}$	10	Silt in sediment [mg silt/L]
$Q(POM_R)_s = -J^{res}_{POM_{R_s}} + J^{dep}_{POM_{R_w}} - J^{deg}_{POM_{R_s}}$	11	Refractory POM in sediment [mg OM/L]
$Q(POM_L)_s = J^{dep}_{POM_{L_w}} - J^{res}_{POM_{L_s}} - J^{deg}_{POM_{L_s}}$	12	Labile POM in sediment [mg OM/L]

Table 2: Mass balances for silt, refractory POM, and labile POM in water and sediment

Subroutine name	*Subroutine operations*
`merc_water.f`	Partitioning, transformations, and sinking of Hg species in water. Gaseous exchange of Hg^0.
`merc_sed.f`	Partitioning, transformations, resuspension, and diffusion of Hg species in the seabed.
`merc_water4sed.f`	Sinking of organic and inorganic particles from the water column. Production of POM_L and degradation of POM_L and POM_R in the water.
`merc_sed4sed.f`	resuspension of organic and inorganic particles from the seabed. degradation of POM_L and POM_R in the seabed. Evolution of the sediment active layer depending on net erosion/deposition.
`mercury.f`	Initial conditions for Hg and sediment state variables. Integration among the merc_ subroutines and with the hydrodynamic model. Mask handling.

Table 3: Subroutines of the Hg model

`what2 = 's4mercury'`
In the the subroutine `mercury.f`, it is also possible to enable restart files with the logical operator `merc_has_restart=.True.`

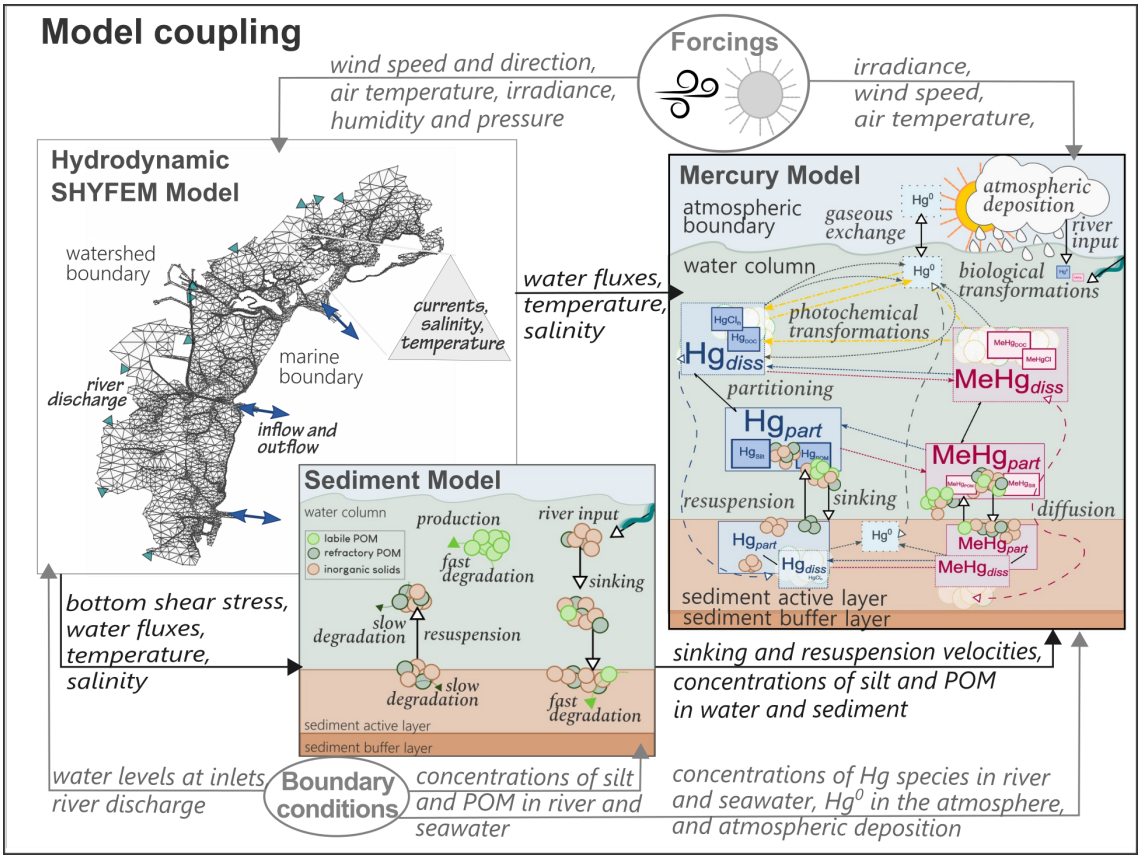

Figure 1: Coupling scheme for the hydrodynamic model with the Hg and sediment model. The left figure synthesizes the main Hg dynamics simulated in the model. Oxidized Hg (Hg^{II}) and methylmercury (MeHg) distribute among dissolved and particulate phases based on partition coefficients $K_{D_{Hg_i-P_i}}$. Transformations (dashed arrows) include photochemical (photoreduction, photooxidation, and photodemethylation) and biological (methylation, demethylation, reduction, and oxidation) processes. Gaseous elemental Hg (Hg^0) is exchanged with the atmosphere depending on turbulence and concentration gradient. Other transport processes include atmospheric deposition, river input, and exchanges driven by hydrodynamics, sediment deposition, and resuspension.

1.2 The mercury module

The evolution of Hg^0 concentrations in water (Reaction 1) is described as the sum of gaseous exchange with the atmosphere ($J^{evs}_{Hg^0}$), diffusion exchange with the sediment ($J^{diff}_{Hg^0}$), and the transformations involving Hg^0 as a sink or source species ($J^{bgc}_{Hg^0_w}$). The evolution of Hg^{II} concentrations in water (Reaction 2) is driven by the sum of the transformations involving Hg^{II} ($J^{bgc}_{Hg^{II}_w}$), diffusion ($J^{diff}_{Hg^{II}}$) of the dissolved species, and resuspension ($J^{res}_{Hg^{II}_s}$) and deposition ($J^{dep}_{Hg^{II}}$) of the particulate species. Similar processes control the evolution of MeHg concentrations (Reaction 3). Hg^0 in sediment (Reaction 4) can be produced through microbial transformations ($J^{bgc}_{Hg^0_s}$) and diffuses across the sediment-water interface. The evolution of Hg^{II} and $MeHg$ in sediment (Reactions 5 and 6) also depend on transformations and diffusion processes, as well as on the resuspension and deposition of their particulate fractions.

The fraction of each particulate or dissolved Hg species (Table 4) is estimated from the concentrations of the various phases (silt, POM_{ref}, POM_{lab}, DOC, kg l^{-1}) and the partitioning coefficients $K_{D_{Hg_i-P_i}}$ (l kg^{-1}) corrected for the porosity of the medium (ϕ_s or ϕ_w) assuming the thermodynamic equilibrium [1, 2].

The exchange of gaseous elemental mercury (Hg^0) between surface waters and the atmosphere (Table 7) depends on the concentration gradient between the two media ($Hg^0_w - Hg^0_{atm}$) corrected for the dimensionless Henry's constant

		Hg species partitioning
$Hg_T = Hg_{Tdiss} + Hg_{Tpart}$	13	Total Hg
$Hg_{Tdiss} = Hg^{II}_{diss} + MeHg_{diss} + Hg^0$	14	Total dissolved Hg species
$Hg_{Tpart} = Hg^{II}_{part} + MeHg_{part}$	15	Total particulate Hg species
$Hg^{II}_{diss} = Hg^{II}_{DOC} + HgCl_n$	16	Dissolved oxidized Hg
$MeHg_{diss} = MeHg_{DOC} + MeHgCl$	17	Dissolved methylated Hg
$Hg^{II}_{part} = Hg^{II}_{silt} + Hg^{II}_{POM_{ref}} + Hg^{II}_{POM_{lab}}$	18	Particulate oxidized Hg
$MeHg_{part} = MeHg_{silt} + MeHg_{POM_{ref}} + MeHg_{POM_{lab}}$	19	Particulate methylated Hg
$HgCl_{n(j)} = [Hg^{II}]_j \cdot f_{aq1(j)}$	20	Hg^{II} complexed to chlorides
$Hg^{II}_{DOC(j)} = [Hg^{II}]_j \cdot f_{doc1(j)}$	21	Hg^{II} complexed to DOC
$MeHgCl_{(j)} = [MeHg]_j \cdot f_{aq2(j)}$	22	MeHg complexed to chlorides
$MeHg_{DOC(j)} = [MeHg]_j \cdot f_{doc2(j)}$	23	MeHg complexed to DOC
$Hg^{II}_{silt(j)} = [Hg^{II}]_j \cdot f_{silt1(j)}$	24	Hg^{II} adsorbed to silt
$Hg^{II}_{POM_{ref}(j)} = [Hg^{II}]_j \cdot f_{POM_{ref}1(j)}$	22	Hg^{II} adsorbed to refractory POM
$Hg^{II}_{POM_{lab}(j)} = [Hg^{II}]_j \cdot f_{POM_{lab}1(j)}$	25	Hg^{II} adsorbed to labile POM
$MeHg_{silt(j)} = [MeHg]_j \cdot f_{silt2(j)}$	26	MeHg adsorbed to silt
$MeHg_{POM_{ref}(j)} = [MeHg]_j \cdot f_{POM_{ref}2(j)}$	27	MeHg adsorbed to refractory POM
$MeHg_{POM_{lab}(j)} = [MeHg]_j \cdot f_{POM_{lab}2(j)}$	28	MeHg adsorbed to labile POM
$f_{aq1(j)} = 1/\big(C_{C_{silt_{(j)}}} \cdot K'_{D_{Hg-silt}} + C_{C_{POM_{lab(j)}}} \cdot K'_{D_{Hg-POM_{lab}}} + + C_{C_{POM_{ref(j)}}} \cdot K'_{D_{Hg-POM_{ref}}} + C_{DOC_{(j)}} \cdot K'_{D_{Hg-DOC}} + 1\big)$	29	Fraction of Hg^{II} complexed to chlorides in the element j (water or sediment)
$f_{aq2(j)} = 1/\big(C_{silt_{(j)}} \cdot K'_{D_{MeHg-silt}} + C_{POM_{lab(j)}} \cdot K'_{D_{MeHg-POM_{lab}}} + + C_{POM_{ref(j)}} \cdot K'_{D_{MeHg-POM_{ref}}} + C_{DOC_{(j)}} \cdot K'_{D_{MeHg-DOC}} + 1\big)$	30	Fraction of MeHg complexed to chlorides in the element j (water or sediment)
$f_{doc1(j)} = \big(C_{DOC_{(j)}} \cdot K'_{D_{Hg-DOC}}\big)/\big(C_{silt_{(j)}} \cdot K'_{D_{Hg-silt}} + C_{POM_{lab(j)}} \cdot K'_{D_{Hg-POM_{lab}}} + C_{POM_{ref(j)}} \cdot K'_{D_{Hg-POM_{ref}}} + C_{DOC_{(j)}} \cdot K'_{D_{Hg-DOC}} + 1\big)$	31	Fraction of Hg^{II} complexed to Dissolved Organic Carbon in the element j (water or sediment)
$f_{doc2(j)} = \big(C_{DOC_{(j)}} \cdot K'_{D_{MeHg-DOC}}\big)/\big(C_{silt_{(j)}} \cdot K'_{D_{MeHg-silt}} + C_{POM_{lab(j)}} \cdot K'_{D_{MeHg-POM_{lab}}} + POM_{ref(j)} \cdot K'_{D_{MeHg-POM_{ref}}} + C_{DOC_{(j)}} \cdot K'_{D_{MeHg-DOC}} + 1\big)$	32	Fraction of MeHg complexed to Dissolved Organic Carbon in the element j (water or sediment)
$f_{silt1(j)} = \big(C_{silt_{(j)}} \cdot K'_{D_{Hg-silt}}\big)/\big(C_{silt_{(j)}} \cdot K'_{D_{Hg-silt}} + C_{POM_{lab(j)}} \cdot K'_{D_{Hg-POM_{lab}}} + C_{POM_{ref(j)}} \cdot K'_{D_{Hg-POM_{ref}}} + C_{DOC_{(j)}} \cdot K'_{D_{Hg-DOC}} + 1\big)$	33	Fraction of Hg^{II} adsobed to silt in the element j (water or sediment)

Table 4: Partitioning of Hg species.

$f_{silt2(j)} = \left(C_{silt_{(j)}} \cdot K^{'}_{D_{MeHg-silt}}\right)/\left(C_{silt_{(j)}} \cdot K^{'}_{D_{MeHg-silt}} + C_{POM_{lab(j)}} \cdot K^{'}_{D_{MeHg-POM_{lab}}} + C_{POM_{ref(j)}} \cdot K^{'}_{D_{MeHg-POM_{ref}}} + C_{DOC_{(j)}} \cdot K^{'}_{D_{MeHg-DOC}} + 1\right)$	34	Fraction of MeHg adsobed to silt in the element j (water or sediment)
$f_{POM_{ref}1(j)} = \left(C_{POM_{ref(j)}} \cdot K^{'}_{D_{Hg-POM_{ref}}}\right)/\left(C_{silt_{(j)}} \cdot K^{'}_{D_{Hg-silt}} + C_{POM_{lab(j)}} \cdot K^{'}_{D_{Hg-POM_{lab}}} + C_{POM_{ref(j)}} \cdot K^{'}_{D_{Hg-POM_{ref}}} + C_{DOC_{(j)}} \cdot K^{'}_{D_{Hg-DOC}} + 1\right)$	35	Fraction of Hg^{II} adsobed to refractory POM in the element j (water or sediment)
$f_{POM_{ref}2(j)} = \left(C_{POM_{ref(j)}} \cdot K^{'}_{D_{MeHg-POM_{ref}}}\right)/\left(C_{silt_{(j)}} \cdot K^{'}_{D_{MeHg-silt}} + C_{POM_{lab(j)}} \cdot K^{'}_{D_{MeHg-POM_{lab}}} + C_{POM_{ref(j)}} \cdot K^{'}_{D_{MeHg-POM_{ref}}} + C_{DOC_{(j)}} \cdot K^{'}_{D_{MeHg-DOC}} + 1\right)$	36	Fraction of MeHg adsobed to refractory POM the element j (water or sediment)
$f_{POM_{lab}1(j)} = \left(C_{POM_{lab(j)}} \cdot K^{'}_{D_{Hg-POM_{lab}}}\right)/\left(C_{silt_{(j)}} \cdot K^{'}_{D_{Hg-silt}} + C_{POM_{lab(j)}} \cdot K^{'}_{D_{Hg-POM_{lab}}} + C_{POM_{ref(j)}} \cdot K^{'}_{D_{HgPOM_{ref}}} + C_{DOC_{(j)}} \cdot K^{'}_{D_{Hg-DOC}} + 1\right)$	37	Fraction of Hg^{II} adsobed to labile POM in the element j (water or sediment)
$f_{POM_{lab}2(j)} = \left(C_{POM_{lab(j)}} \cdot K^{'}_{D_{MeHg-POM_{lab}}}\right)/\left(C_{silt_{(j)}} \cdot K^{'}_{D_{MeHg-silt}} + C_{POM_{lab(j)}} \cdot K^{'}_{D_{MeHg-POM_{lab}}} + C_{POM_{ref(j)}} \cdot K^{'}_{D_{MeHg-POM_{ref}}} + C_{DOC_{(j)}} \cdot K^{'}_{D_{MeHg-DOC}} + 1\right)$	38	Fraction of MeHg adsobed to labile POM the element j (water or sediment)
$K^{'}_{D_{Hg_i-P_i}} = \frac{K_{D_{Hg_i-P_i}}}{\phi_j}$	39	Partition coefficient for the Hg species i to the phase P_i corrected to the porosity of the medium ϕ_j
$C_{P_{i(j)}} = P_{i(j)} \cdot 10^{-6}$	40	Concentrations of silt, POM_R, POM_L, and DOC in the element j (water or sediment)

Table 4: (continued) Partitioning of Hg species.

$J^{bgc}_{Hg^0_w} = J^{bred}_{Hg^{II}_w} + J^{opm}_{Hg^{II}_w} + J^{rdem}_{MeHg_w} + -J^{box}_{Hg^0_w} + J^{phrd}_{Hg^{II}_w} - J^{phox}_{Hg^0_w} + \alpha\, J^{phdem}_{MeHg_w}$	41	Transformations for Hg^0 in water
$J^{bgc}_{Hg^{II}_w} = J^{dem}_{(MeHg_w} - J^{met}_{Hg^{II}_w} - J^{bred}_{Hg^{II}_w} + -J^{opm}_{Hg^{II}_w} + J^{box}_{Hg^0_w} + J^{phox}_{Hg^0)_w} - J^{phrd}_{Hg^{II}_w} + (1-\alpha)\, J^{phdem}_{MeHg_w}$	42	Transformations for Hg^{II} in water
$J^{bgc}_{MeHg_w} = J^{met}_{Hg^{II}_w} - J^{dem}_{MeHg_w} - J^{rdem}_{MeHg_w} - J^{phdem}_{MeHg_w}$	43	Transformations for MeHg
$J^{bgc}_{Hg^0_s} = J^{opm}_{Hg^{II}_s} + J^{rdem}_{MeHg_s}$	44	Transformations for Hg^0 in sediment
$J^{bgc}_{Hg^{II}_s} = J^{dem}_{MeHg_s} - J^{met}_{Hg^{II}_s} - J^{opm}_{Hg^{II}_w}$	45	Transformations for Hg^{II} in sediment
$J^{bgc}_{MeHg_s} = J^{met}_{Hg^{II}_s} - J^{dem}_{MeHg_s} - J^{rdem}_{MeHg_s}$	46	Transformations for MeHg in sediment
$J^{met}_{Hg^{II}_s} = k_{met_s} \cdot Q_b^{\frac{T-20}{10}} \cdot \left[Hg^{II}_{diss}\right]_s$	47	Methylation of Hg^{II} in sediment
$J^{dem}_{MeHg_s} = k_{dem_s} \cdot e^{\left(E_a \cdot 10^3 \cdot \frac{T_k - 293}{R_{cal} \cdot T_k \cdot 293}\right)} \cdot \left[MeHg_{diss}\right]_s$	48	Oxidative demethylation of MeHg in sediment
$J^{met}_{Hg^{II}_w} = k_{met_w} \cdot Q_b^{\frac{T-20}{10}} \cdot \left[Hg^{II}_{diss} + Hg^{II}_{POM_{ref}(j)} + Hg^{II}_{POM_{lab}(j)}\right]_w$	49	Methylation of Hg^{II} in water
$J^{dem}_{MeHg_w} = k_{dem_w} \cdot e^{\left(E_a \cdot 10^3 \cdot \frac{T_k - 293}{R_{cal} \cdot T_k \cdot 293}\right)} \cdot \left[MeHg_{diss} + MeHg_{POM_{ref}(j)} + MeHg_{POM_{lab}(j)}\right]_w$	50	Oxidative demethylation of MeHg in water
$J^{phox}_{Hg^0_w} = k_{phox} \cdot I_0 \cdot e^{(-k_e \cdot z)} \cdot \left[Hg^0\right]_w$	51	Photochemical oxidation of Hg^0 in water
$J^{phred}_{Hg^{II}_w} = k_{phred} \cdot I_0 \cdot e^{(-k_e \cdot z)} \cdot \left[Hg^{II}_{diss}\right]_w$	52	Photochemical reduction of Hg^{II} in water
$J^{phdem}_{MeHg_w} = k_{phdem} \cdot PAR \cdot e^{(-k_e \cdot z)} \cdot \left[MeHg_{diss}\right]_w$	53	Photochemical demethylation of MeHg in water
$J^{opm}_{Hg^{II}_j} = k_{opm_j} \cdot \left[Hg^{II}_{diss}\right]_j$	54	Reduction of Hg^{II} mediated by the mer-operon in water and sediment
$J^{rdem}_{MeHg_j} = k_{opm_j} \cdot \left[MeHg_{diss}\right]_j$	55	MeHg demethylation mediated by the mer-operon in water and sediment
$J^{bred}_{Hg^{II}_w} = k_{bred_w} \cdot Q_{b2}^{\frac{T-25}{10}} \cdot \left[Hg^{II}_{diss} + Hg^{II}_{POM_{lab}}\right]_w$	56	Biological reduction of Hg^{II} in water
$J^{box}_{Hg^0_w} = k_{box_w} \cdot Q_{b2}^{\frac{T-25}{10}} \cdot \left[Hg^0\right]_w$	57	Dark oxidation of Hg^0 in water

Table 5: Functional Expression for Transformations of Hg Species.

$J^{diff}_{Hg^0} = \frac{D_{(Hg^0)} \cdot \phi_s}{Z_s \cdot \xi_s} \cdot \left\{ [Hg^0]_w - [Hg^0]_s \right\}$	58	Pore water Diffusion of Hg^0
$J^{diff}_{Hg^{II}} = \frac{D_{(HgII)} \cdot \phi_s}{Z_s \cdot \xi_s} \cdot \left\{ \left[Hg^{II}_{diss}\right]_w - \left[Hg^{II}_{diss}\right]_s \right\}$	59	Pore water Diffusion of Hg^{II}
$J^{diff}_{MeHg} = \frac{D_{(MeHg)} \cdot \phi_s}{Z_s \cdot \xi_s} \cdot \left\{ \left[MeHg_{diss}\right]_w - \left[MeHg_{diss}\right]_s / \phi_s \right\}$	60	Pore water Diffusion of MeHg
$J^{Res}_{Hg^{II}_s} = v_r \cdot \left[Hg^{II}_{part}\right]_{sed}$	61	Resuspension of particulate Hg^{II} from sediment
$J^{Res}_{MeHg_s} = v_r \cdot \left[MeHg_{part}\right]_{sed}$	62	Resuspension of particulate MeHg from sediment
$J^{Dep}_{Hg^{II}_w} = v_d \cdot \left[Hg^{II}_{part}\right]_w$	63	Deposition of particulate Hg^{II} from water
$J^{Dep}_{MeHg_w} = v_d \cdot \left[MeHg_{part}\right]_w$	64	Deposition of particulate MeHg from water
$\xi_s = \sqrt{1 - ln(\phi_s^2)}$	65	Sediment tortuosity
ϕ_s (Table 9)	66	Sediment porosity
v_r (Table 9)	67	Resuspension velocity
v_d (Table 9)	68	Deposition velocity

Table 6: Functional Expression for Sediment-Water exchanges of Hg species.

$Evs_{(Hg^0)} = k_w \cdot \left\{ [Hg^0]_w - [Hg^0]_{atm} / k_{H'} \right\}$	69	Gaseous exchange of Hg^0
$k_w = 0.1 + 2.26 \cdot u_{w10} \cdot \left(\frac{Sc_{(Hg)}}{Sc_{(CO_2)}}\right)^{-0.5}$	70	Volatilization rate constant
$k_{H'} = exp(\frac{-2403.3}{T_k} + 6.92) \cdot 0.016$	71	Dimensionless Henry's law constant
$Sc_{(CO_2)} = 0.11 \cdot (T^2) - 6.16 \cdot T + 644.7$	72	Schmidt number for CO_2
$Sc_{(Hg^0)} = \nu / D_{Hg^0}$	73	Schmidt number for Hg^0
$\nu = \frac{\mu_w}{\rho_w} \cdot 10^3$	74	Kinematic viscosity of water
$D_{(Hg^0)} = \frac{7.4 \cdot 10^{-8} (s_w \cdot M_w)^{1/2} \cdot T}{\mu_w \cdot Molv^{0.6}_{(Hg)}}$	75	Diffusivity for Hg^0
$\mu_w = (1.791 - T \cdot (0.06144 - T \cdot (0.001451 - T \cdot 0.000016826)) - 0.0001529 \cdot 1.013253 + 0.000000083885 \cdot 1.013253^2 + 0.0024727 \cdot Sal + (0.0000060574 \cdot 1.013253 - 0.000000002676 \cdot 1.013253^2) \cdot T + ((T \cdot 0.000048429 - T \cdot (0.0000047172 - T \cdot 0.000000075986)) \cdot Sal))/10^3$	76	Dynamic Water viscosity
$\rho_w = 999.842594 + 0.06793952 \cdot T - 0.00909529 \cdot (T^2) + 1.00168d - 4 \cdot T^3. - 1.120083d - 6 \cdot T^4. + 6.536332d - 9 \cdot T^5 + (0.824493 - 0.0040899 \cdot T + 0.000076438 \cdot (T^2) - 8.2467d - 7 \cdot T^3 + 5.3875d - 9 \cdot T^4) \cdot Sal + (-0.00572466 + 0.00010227 \cdot T - 1.6546d - 6 \cdot (T^2)) \cdot Sal^{1.5} + 0.00048314 \cdot (Sal^2)$	77	Water density

Table 7: Functional Expression for gaseous exchange of Hg^0.

for Hg^0 ($k_{H'}$) and the transfer velocity of the gas (k_w), which is estimated through empirical formulations taking into account wind speed (u_{w10}) and the Schmidt numbers for Hg^0 and CO_2 (Sc_{Hg^0} and Sc_{CO_2}). Sc_{CO_2} and $k_{H'}$ in turn depend on water temperature, and Sc_{Hg^0} is calculated from water viscosity and diffusivity of Hg^0 [7]. Atmospheric Hg (Hg^0_{atm}) is set at a fixed concentration, and wind speed is a model forcing. The model employs for k_w (Reaction 68) the formulation for microtidal estuaries estimated by [8].

The transformations driving the inter-conversion among Hg species ($J^{bgc}_{Hg_{ij}}$) are described by first-order kinetics (Table 5). They include photochemical transformations (photo-reduction, photo-oxidation, photo-demethylation) and biological transformations (Hg methylation and demethylation, biological reduction and oxidation, mer-operon mediated transformations).

Hg methylation and oxidative demethylation of MeHg (i.e., yielding Hg^{II}) are assumed to occur both in water [9, 10] and seabed [11, 12]. In the seabed, these two processes are assumed to involve only the dissolved Hg species (Reactions 47 and 48). In the water, methylation and demethylation in sinking particles have been observed [13, 14], thus they are assumed to involve both dissolved and POM-adsorbed Hg species (Reactions 49 and 50). To take into account the effect of temperature increase on bacterial activity, the rate constant for Hg methylation is corrected for the term Q_B, while for demethylation a bacterial activation energy parameter (E_a) is used [2, 4].

Photo-oxidation (Reaction 51), photo-reduction (Reaction 52), and photo-demethylation (Reaction 53) of dissolved Hg species in water depend on light availability (I_0) attenuated for the extinction coefficient (k_e) and water depth (z_w).

In polluted environments, the microbial community usually displays genes for resistance to Hg, clustered in the mer operon. Depending on the configuration of the mer operon, these genes can promote either solely Hg^{II} reduction (narrow-spectrum resistance), or both Hg^{II} reduction and reductive demethylation of MeHg (broad-spectrum resistance) [15]. In the model, broad-spectrum resistance is parameterized both in water and sediment (Reactions 54 and 55), with an activation threshold at $Hg_{T_{diss}}$= 50 pM (10 ng l^{-1}) [16].

Biological reduction of Hg^{II} can also be mediated by phytoplankton through a plethora of different pathways [17] as well as by bacteria at ambient levels [18, 19]. Here the process (Reaction 56) is assumed to be temperature dependent [9, 18, 19] and to involve both dissolved Hg^{II} and Hg^{II} complexed to labile POM. Biological oxidation of Hg^0 (Reaction 57), promoted by algal biogenic material [20] is also assumed to be temperature dependent.

Diffusion fluxes ($J^{pwd}_{Hg_i}$) of dissolved Hg species (Hg^{II}_{diss}, $MeHg_{diss}$, and Hg^0) at the sediment-water interface are modeled following Fick's Law (Reactions 58-60). They depend on the concentration gradient and the diffusion coefficient (D_{Hg_i}) for Hg and MeHg, corrected for sediment thickness (Z_s), porosity (ϕ_s), and tortuosity (ξ_s) [21].

Fluxes of particulate Hg species (Hg^{II}_{part} and $MeHg_{part}$) between sediment and water are driven by resuspension ($J^{res}_{Hg_{i_s}}$, Reactions 61-62) and deposition ($J^{dep}_{Hg_{iw}}$, Reactions 63-64) according to the deposition and resuspension velocities computed in the sediment module.

The initial conditions for Hg^{II} and MeHg in sediment must be set in units of $\mu g\, g^{-1}$, as usually available from field studies. The concentrations are internally converted to volumetric concentrations ($\mu g\, m^{-3}$) of particulate and dissolved fractions taking into account the mass of sediments in the seabed, the sediment porosity, and the average partition coefficient ($\overline{K}_D$), as shown in Table 8 [22]. At the first iteration, the value of $[Hg_i]_{s(t_0)}$ (Reaction 78) is re-partitioned based on the Equations of Table 4 and updated based on the reactions of Table 1. In the following iterations $[Hg_i]_{s(t_0)}$ is not used anymore, and the evolution of concentrations is driven only by model processes. For Hg^0 it is recommended to initialize sediment values at 0, and let the concentrations build up in pore-water due to diffusion and transformation processes.

$[Hg_{i_{part}}]_{s(t_0)} = [Hg_{i_{\mu gg}}]_s \cdot (silt + POM_R)$	78	Volumetric concentration ($\mu g\, m^{-3}$) of particulate Hg species for seabed initialization
$[Hg_{i_{diss}}]_{s(t_0)} = [Hg_{i_{\mu gg}}]_s \cdot \phi_s / \overline{K}_D$	79	Volumetric concentration ($\mu g\, m^{-3}$) of Hg species dissolved in pore-water for seabed initialization
$[Hg_i]_{s(t_0)} = [Hg_{i_{part}}]_{s(t_0)} + [Hg_{i_{diss}}]_{s(t_0)}$	80	Volumetric concentration ($\mu g\, m^{-3}$) of Hg species (dissolved and particulate) for seabed initialization
$\overline{K}_D = (K_{D_{Hg_i-silt}} \cdot silt + K_{D_{Hg_i-POM_R}} \cdot POM_R)/(silt + POM_R)$	81	Average partition coefficient for the Hg species Hg_i
$[Hg_{i_{\mu gg}}]_s$	82	Mass of Hg species per unit mass of dry solids ($\mu g\, g^{-1}$) (*input*)

Table 8: Equations for the initialization of Hg^{II} and MeHg in sediment

1.3 The sediment module

The sediment module simulates three state variables representative of different kinds of sediment: fine inorganic particles (*silt*), refractory organic matter (POM_{ref}), and labile organic matter (POM_{lab}). POM_{lab} represents the plankton component in a simplified fashion and POM_{ref} represents the organic matter of terrestrial origin. POM_{lab} is produced in the water as a function of temperature and is degraded at a fast pace, while POM_{ref} enters the water through river input and sediment resuspension, and has a long turnover time (Table 12) [23].

Silt and POMs are dynamically exchanged between the water column and the seabed (Table 9) depending on sediment properties and the bottom shear stress (τ_b), which is computed by the hydrodynamic model [24]. Particles resuspension from the seabed occurs when τ_b is higher than the critical threshold for sediment erosion (τ_{ce}). Sinking from the water column to the seabed occurs when τ_b is lower than the critical threshold for sediment deposition (τ_{cd}) [25].

The deposition flux of each sediment state variable ($J^{dep}_{P_i,w}$) is described by Reaction 83 [26], where $[P_i]_w$ is the water concentration of a given state variable (silt, POM_{lab}, or POM_{ref}) and v_d is the deposition velocity. The deposition velocity depends on the probability of deposition P_d and the settling velocity, which is calculated from particles diameters (d_{P_i}, m), particle density (ρ_P), water density (ρ_w), and water viscosity (μ_w) following Stoke's law.

The erosion flux of surface sediment is described by Reaction 84 [27]. Sediment erodability is parameterized through an erosion rate coefficient ϵ_M (Reaction 91, in mg cm^{-2} h^{-1}) that depends on the wet bulk density of the seabed (ρ_b) [27]. The erosion flux is calculated for the surface layer in its entirety and distributed among the three sediment state variables depending on their relative abundances (Reactions 93 - 95).

Sediment wet bulk density (Reaction 100) is obtained from porosity (ϕ_s) and sediment dry density (ρ_d), which are calculated from the seabed organic carbon content following the equations for flooded sediment described in [28]. In particular, sediment dry density (ρ_d) is calculated from the content of organic carbon in sediment in mg g^{-1} (Reaction 101), and the average density of sediment particles (ρ_s, Reaction 102) is corrected to account for to the POM%. Sediment porosity is estimated by combining these two properties (Reaction 103).

This simplified representation of the seabed offers the advantage to require as input only the sediment content of organic carbon (OC%), which is routinely monitored in environmental studies, and a limited number of other parameters (Table 12). The limitation given by the absence of non-cohesive sandy sediments in the model is overcome by setting spatial variable values for the critical threshold for sediment erosion (τ_{ce}) differentiating this parameter for the inlets, the internal channels, and the shallow areas. The values of τ_{ce} can be modified in the subroutine `mercury.f`. Moreover, the sheltering effect of landforms and benthic vegetation [29] can be reproduced by masking the values of the bottom shear stress in the areas of concern, reducing them to zero (see Section 1.4). In this way, sediment resuspension is suppressed, while deposition is maximum.

Initial conditions for sediment are given as OC% (Reaction 105), and the model internally calculates the concentrations of silt and POMs assuming that at the first iteration all the POM in the sediment is refractory. The composition and the

$J^{dep}_{P_{i,w}} = v_{d_{(P_i)w}} \cdot \left[P_i\right]_w$	83	Sediment deposition flux for the state variable P_i in water
$J^{res}_{P_{i,s}} = \epsilon_M \cdot \left(\frac{\tau_b - \tau_{ce}}{\tau_{ce}}\right)^2 \cdot \frac{P_{i,s}}{\sum P_{i,s}} \cdot \frac{\left[P_i\right]_s}{\left[P_i\right]_s + 0.00001}$	84	Sediment erosion flux or the state variable P_i in sediment
$J^{PP}_{POM_{lab,w}} = k_{pp_{POM_{lab,w}}} \cdot 1.2^{(T-20)}$	85	Production of POM_{lab} in the water
$J^{deg}_{POM_{ref,j}} = k_{deg_{POM_{ref,j}}} \cdot 1.05^{(T-20)} \cdot POM_{ref}$	86	Degradation of POM_{ref} in sediment and water
$J^{deg}_{POM_{lab,j}} = k_{deg_{POM_{lab,j}}} \cdot 1.05^{(T-20)} \cdot POM_{lab}$	87	Degradation of POM_{lab} in sediment and water
$v_{d_{(P_i)w}} = v_{s_{(P_i)w}} \cdot P_d$	88	Deposition velocity for the sediment state variable P_i
$v_{s_{(P_i)w}} = \frac{g}{18 \cdot \mu_w} \cdot (\rho_{(P_i)} - \rho_w) \cdot d^2_{(P_i)}$	89	Settling velocity for the sediment state variables P_i
$P_d = \begin{cases} 0 & \text{if} \quad \tau_b > \tau_{cd} \\ \frac{\tau_{cd} - \tau_b}{\tau_{cd}} & \text{if} \quad \tau_b < \tau_{cd} \end{cases}$	90	Probability of deposition
$\epsilon_M = \begin{cases} 0 & \text{if} \quad \tau_b < \tau_{ce} \\ 10^{0.23 \cdot \exp\left(\frac{0.198}{\rho_b - 1.0023}\right)} & \text{if} \quad \tau_b > \tau_{ce} \end{cases}$	91	Base erosion rate per unit surface area
$v_r = \frac{\sum J^{res}_{P_{i,s}}}{\sum P_{i,s}}$	92	Resuspension velocity
$POM\% = \begin{cases} 1.7 \cdot OC\% & if \quad t = 0 \\ \frac{POM_{ref} + POM_{lab}}{\sum P_{i,s}} & if \quad t > 0 \end{cases}$	97	Percentage of POM in sediment
$\rho_b = \phi_s + \rho_d$	100	Bulk density of the seabed
$\rho_d = 1.776 \ - \ 0.363 \cdot log_n(OC_{mgg})$	101	Dry density of the seabed
$\rho_s = 1.25 POM\% + 2.65 \cdot (100 - POM\%)$	102	Average density of sediment particles in the seabed
$\phi_s = 1 - \frac{\rho_d}{\rho_s}$	103	Sediment porosity
$OC_{mgg} = 0.1 \cdot OC\%$	104	Organic carbon in the seabed
$OC\% = \begin{cases} input & if \quad t = 0 \\ POM\%/1.7 & if \quad t > 0 \end{cases}$	105	Percentage of organic carbon in sediment
$\frac{dZ_s}{dt} = \left(\frac{J^{dep}_{silt,w} - J^{res}_{silt}}{\rho_{silt}} + \frac{J^{dep}_{POM_{ref}} - J^{res}_{POM_{ref}} - J^{deg}_{POM_{ref}}}{\rho_{POM_{ref}}} + \frac{J^{dep}_{POM_{lab}} - J^{res}_{POM_{lab}} - J^{deg}_{POM_{lab}}}{\rho_{POM_{lab}}}\right) \cdot \frac{1}{1-\phi}$	106	Variation of the sediment thickness

Table 9: Functional Expression Description for Dynamics of Sediment State Variables P_i (silt, POM_{ref}, and POM_{lab}).

T	(C)	Water temperature in Celsius
I_0	(W m^{-2})	Incident light intensity at the surface
z	(m)	Depth
u_{w10}	(m sec^{-1})	Wind speed
τ_b	(Pa)	Bottom shear stress
Sal	(-)	Salinity
Vol	(m^3)	Volume
$T_k = T + 273.15$	(K)	Water temperature in Kelvin
$PAR = I_0 \cdot 0.432$	(E m^{-2} d^{-1})	Photosynthetic active radiation

Table 10: Imported and Derived Variables.

thickness (Z_s) of the surface sediment layer vary during the simulation (Reaction 106) in response to deposition, erosion, and degradation of particles [30]. If net deposition occurs, the surface layer increases in thickness, while in the case of net erosion, the thickness is reduced up to a threshold value (Z_0), at which the initial thickness ($Z_{s(IN)}$) is restored incorporating the sediment from the subsurface layer, which is maintained constant throughout the simulation [31].

The model is initialized with a default spatially homogeneous value of OC%=2, which can be modified either from the flag `esolsinit` in the subroutine `mercury.f` or by providing an external file in fem format (see Section 1.4) with spatially variable values of OC% followed by two dummy variables.

1.4 Parameters for the str file

Below the parameters to set in the input file `str`:
`imerc` = 1 simulates mercury dynamics in water and seabed
`issedi` = 1 simulates particles dynamics in water and seabed

To set boundary conditions add to the section `$bound`:
`mercn` = file name that contains boundary conditions for Hg state variables.
`s4mern` = file name that contains boundary conditions for particles state variables.
The format is the same as for the file `boundn`, which is required, along with the file `tempn`, to run the Hg model. The first column is for the date and the following columns (3 data columns for Hg, and 3 data columns for sediment) must have the same unit as the corresponding variable.

The model allows to use spatially variable initial conditions for the concentrations of Hg species and for the sediment variables in water and sediment. The initialization files must be in the `.fem` format containing the field values on a georeferenced grid. The name of the different initialization files must be indicated in the `$name` section of the `.str` file using the following flags:
`merc_emp`: initialization file defining the concentration values of Hg^{II}, MeHg, and Hg^0 in the water.
`merc_ems`: initialization file defining the concentration values of Hg^{II} and MeHg in the sediment.
`merc_solw`: initialization file defining the concentration values of silt, POM_{ref}, and POM_{lab} .
`merc_sols`: initialization file defining the percentage of organic carbon in the sediment (OC%).
When an external file is not provided, the spatially homogeneous default values encoded in the `mercury.f` subroutine are used for the concerned variables.

The mask to be applied to the bottom shear stress to account for the sheltering effect of landforms and benthic vegetation can be provided through another file `.fem` containing a field of integers defined on a georeferenced grid. The field must contain the values of the mask, equal to zero in the regions where the sheltering effect must be applied, and equal to one anywhere else. The name of the mask file can be indicated in the `$name` section of the `.str` file using the flag `merc_mask`.

$K_{D_{Hg-silt}} = 2.5 \cdot 10^5$	(l kg^{-1})	Partition coefficient of Hg^{II} to silt	[32, 33]
$K_{D_{Hg-pomR}} = 10^6$	(l kg^{-1})	Partition coefficient of Hg^{II} to refractory POM	[33]
$K_{D_{Hg-pomL}} = 10^6$	(l kg^{-1})	Partition coefficient of Hg^{II} to labile POM	[33]
$K_{D_{Hg-DOC}} = 10^6$	(l kg^{-1})	Partition coefficient of Hg^{II} to DOC	
$K_{D_{MeHg-silt}} = 2.4 \cdot 10^4$	(l kg^{-1})	Partition coefficient of MeHg to silt	[32, 33]
$K_{D_{MeHg-pomR}} = 10^6$	(l kg^{-1})	Partition coefficient of MeHg to refractory POM	[33]
$K_{D_{MeHg-pomL}} = 10^6$	(l kg^{-1})	Partition coefficient of MeHg to labile POM	[33]
$K_{D_{MeHg-DOC}} = 10^4$	(l kg^{-1})	Partition coefficient of MeHg to DOC	
$k_e = 1.8$	(m^{-1})	Extinction coefficient	
$Q_B = 2.5$	(-)	Temperature coefficient for bacterial methylation	[1]
$Q_{B2} = 2$	(-)	Temperature coefficient for biological reduction and oxidation	[18, 19]
$E_a = 10$	(kcal mol^{-1})	Activation energy for oxidative demethylation	[1]
$R_{cal} = 1.987$	(cal mol^{-1} K^{-1})	Activation energy for oxidative demethylation	[1]
$k_{box_w} = 2.4$	(d^{-1})	Rate constant for biological oxidation in water	[20]
$k_{bred_w} = 0.12$	(d^{-1})	Rate constant for biological reduction in water	[18, 9]
$k_{phox_w} = 0.55$	(d^{-1})	Rate constant for photochemical oxidation in water	[6]
$k_{phred_w} = 0.15$	(d^{-1})	Rate constant for photochemical reduction in water	[6]
$k_{phdem_w} = 0.0025$	(d^{-1})	Rate constant for photochemical demethylation in water	[6]
$k_{met_w} = 0.001$	(d^{-1})	Rate constant for microbial Hg methylation in water	[9]
$k_{dem_w} = 0.01$	(d^{-1})	Rate constant for oxidative demethylation in water	[9, 34]
$k_{met_s} = 0.017$	(d^{-1})	Rate constant for microbial Hg methylation in sediment	[32]
$k_{dem_s} = 0.15$	(d^{-1})	Rate constant for oxidative demethylation in sediment	[11]
$k_{opm_w} = \begin{cases} 0.19 & \text{if Hg}_{Tdiss} > 10 \text{ ng l}^{-1} \\ 0 & \text{if Hg}_{Tdiss} < 10 \text{ ng l}^{-1} \end{cases}$	(d^{-1})	Rate constant for mer-operon mediated Hg^0 production in water	[35, 16]
$k_{opm_s} = \begin{cases} 0.25 & \text{if Hg}_{Tdiss} > 10 \text{ ng l}^{-1} \\ 0 & \text{if Hg}_{Tdiss} < 10 \text{ ng l}^{-1} \end{cases}$	(d^{-1})	Rate constant for mer-operon mediated Hg^0 production in water	[11, 16]

Table 11: Parameters for the mercury module with values for the Venice Lagoon.

$Hg^0_{atm} = 0.0016$	(μg m^{-3})	Concentration of elemental Hg in the atmosphere
$s_w = 2.26$	(-)	Solvent association factor to define the effective molecular weight of the solvent with respect to diffusion
$M_w = 18$	(g mol^{-1})	Molecular weight of water
$Mol_v = 12.74$	(cm^3 mol^{-1})	Molal volume of mercury at its normal boiling temperature

Table 11: (continued) Parameters for the mercury module with values for the Venice Lagoon.

$g = 9.18$	(m s^{-1})	Gravitational constant	
$d_{silt} = 1 \cdot 10^{-5}$	(m)	Silt particle diameter	
$d_{POM_{ref}} = 2 \cdot 10^{-5}$	(m)	POM$_{ref}$ particle diameter	
$d_{POM_{lab}} = 2 \cdot 10^{-5}$	(m)	POM$_{lab}$ particle diameter	
$\rho_{silt} = 2.65$	(g cm^{-3})	Silt particle density	
$\rho_{POM_{ref}} = 1.25$	(g cm^{-3})	POM$_{ref}$ particle density	
$\rho_{POM_{lab}} = 1.016$	(g cm^{-3})	POM$_{lab}$ particle density	
$k_{deg_{(POM_{ref})j}} = 0.00005$	(d^{-1})	Rate constant for POM$_{ref}$ degradation in water and sediment	[23]
$k_{deg_{(POM_{lab})j}} = 0.05$	(d^{-1})	Rate constant for POM$_{lab}$ degradation in water and sediment	[23]
$k_{pp_{(POM_{lab})w}} = 0.33$	(g m^{-3}d^{-1})	Rate constant for POM$_{lab}$ production in water	[2]
$\tau_{cd} = 0.8$	(Pa)	Critical threshold of shear stress for sediment deposition	[31]
$\tau_{ce} = \begin{cases} 0.7 & \text{for inlets and canals} \\ 0.6 & \text{for tidal flats} \end{cases}$	(Pa)	Critical threshold of shear stress for sediment erosion	[36]
$Z_0 = 0.02$	(m)	Critical threshold for seabed thickness at which the initial thickness $Z_{s(IN)}$ is restored	
$Z_{s(IN)} = 0.05$	(m)	Initial thickness of the seabed	

Table 12: Parameters for the sediment module with default values.

2 Supplementary Tables

Boundary	**[Hg^{II}]** pM	**[MeHg]** pM	**[Hg^0]** pM	**L$_{Hg^{II}}$** mol y^{-1}	**L$_{MeHg}$** mol y^{-1}	**L$_{Hg^0}$** mol y^{-1}	**variability**	**Ref.**
Sea	8.72	0.13	0.39	-	-	-	fixed values	[33, 37]
River	54.04 ± 3.9	0.90 ±0.06	0.55 ± 0.04	64.22	1.05	0.65	monthly values	[33]
Atmosphere	-	-	7.9 pmol m^{-3}	54.04	0.27	0	fixed values	[33, 38]
Initial Condition	7.48	0.02	0.09					
Boundary	**[silt]** mg l^{-1}	**[POM$_{ref}$]** mg l^{-1}	**[POM$_{ref}$]** mg l^{-1}	**L$_{silt}$** Mg y^{-1}	**L$_{POM_R}$** Mg y^{-1}	**L$_{POM_L}$** Mg y^{-1}		
Sea	9.25 ± 5.31	0.08 ± 0.06	0.76 ± 0.57	NA	NA	NA	monthly values	[39]
River	2.00	0.20	0.001	2330	233	1	fixed values	
Initial Condition	3.00	1.00	0.00					

Table 13: Boundary and initial conditions used to model Hg dynamics in the Venice lagoon.

	τ_{ce} for shallow areas (<1 m depth)	*τ_{ce} for tidal flats*	*τ_{ce} for channels and inlets*
test1	0.6	0.6	0.6
test2	0.55	0.55	0.55
test3	0.65	0.65	0.65
test4	0.5	0.5	0.5
test5	0.5	0.7	0.6
test6	0.55	0.75	0.65
test7	0.6	0.5	0.65

Table 14: Setup of the simulation for model calibration. Values of τ_{ce} (critical threshold for erosion) are given for different areas of the model domain used in each simulation.

simulation	**ME**	**MAE**	**RMAE**	**RMSE**	**SI**	**r**	**r by station**
test1	-16.88	20.07	0.84	28.54	0.25	n.s.	0.50
test2	-13.63	20.39	0.86	29.98	0.26	0.1	0.53
test3	-19.05	20.43	0.86	28.65	0.26	n.s.	0.43
test4	-8.65	22.02	0.92	35.16	0.29	0.12	0.55
test5	-8.75	22.04	0.93	35.12	0.29	0.12	0.55
test6	-8.65	22.02	0.92	35.16	.029	0.12	0.55
test7	**-16.02**	**19.83**	**0.83**	**28.55**	**0.25**	**n.s.**	**0.54**

Table 15: Statistics calculated to evaluate model performances in simulating suspended organic matter (SPM) (see Section 2.3.1 of the main text and Supplementary equations).

Sensitivity simulation		Hg^{II}_w	$MeHg_w$	Hg^0_w	Hg^{II}_s	$MeHg_s$	Hg^0_{pw}
Sea boundary	+50%	+9.7	+3.7	+10.7	+0.65	+3.71	+0.42%
	-50%	-4.9%	-1.9%	-5.4%	-0.33%	-1.86%	-0.19%
River Hg^{II} boundary	+50%	+1.2%	+0.03%	+1.6%	+0.05%	+0.03%	+0.04%
	- 50%	-1.2%	-0.03%	-1.6%	-0.05%	-0.03%	-0.04%
River MeHg boundary	-50%	~ 0%	-0.61 %	~ 0%	~ 0%	-0.61%	~ 0%
	+50%	~ 0%	+0.61 %	~ 0%	~ 0%	+0.61%	~ 0%
Atmospheric Hg boundary	+50%	+1.7%	+0.27%	+2.4%	+0.07%	+0.7%	+0.05%
	-50%	-0.86%	-0.14%	-1.18%	-0.04%	-0.14%	-0.02%
τ_{ce} (resuspension)	+50%	-76.2%	-12.7%	-68.5%	+3.6%	-0.32%	+0.5%
	-50%	+58.9%	-38.7%	-55.1%	-42.1%	-40.8%	-34.9%
k_{met_w} (water methylation)	+50%	-0.04%	+11.24%	-0.04%	~ 0%	+1.44%	~ 0%
	-50%	+0.04%	-11.21%	-0.04%	~ 0%	-1.45%	~ 0%
k_{met_s} (sediment methylation)	+50%	-0.01%	+4.1%	-0.01%	-0.02%	+11.0%	~ 0%
	-50%	+0.01%	-3.69%	+0.01%	+0.01%	-9.97%	~ 0%
k_{dem_w} (water demethylation)	+50%	+0.01%	+2.7%	+0.02%	~ 0%	+0.29%	~ 0%
	-50%	-0.01%	-2.4%	-0.01%	~ 0%	-0.26%	~ 0%
k_{dem_s} (sediment demethylation)	+50%	~ 0%	-0.24%	~ 0%	~ 0%	-0.58%	~ 0%
	-50%	~ 0%	+0.24%	~ 0%	~ 0%	+0.59%	~ 0%
k_{opm_w} (mer operon reduction water)	+50%	~ 0%	-0.42%	~ 0%	~ 0%	-0.06%	~ 0%
	-50%	~ 0%	+0.44%	~ 0%	~ 0%	+0.07%	~ 0%
k_{opm_s} (mer operon reduction sediment)	+50%	-0.06%	-0.04%	-0.06%	-0.06%	-0.07%	13%
	-50%	+0.21%	0.14%	+0.20%	+0.19%	+0.24%	-49.9%
k_{bred_w} (biotic reduction water)	+50%	-0.60%	-0.37%	+1.6%	-0.04%	-0.04%	-0.02%
	-50%	+0.62%	+0.41%	-1.7%	+0.04%	+0.04%	+0.02%
k_{box_w} (biotic oxidation)	+50%	+1.35%	+0.52%	-3.6%	+0.08%	+0.07%	+0.05%
	-50%	-1.64%	-0.78%	+4.35%	-0.1%	-0.09%	-0.06%
k_{phred_w} (photo-reduction water)	+50%	-10.6%	-2.23%	+27.0%	-0.69%	-0.36%	-0.50%
	-50%	+15.29%	+2.74%	-36.7%	+0.90%	+0.44%	+0.59%
k_{phred_w} (photo-oxidation water)	+50%	+7.7%	1.5%	-18.6%	+0.46%	+0.23%	+0.3%
	-50%	-12.5 %	-2.7%	+31.6%	-0.79%	-0.43%	-0.57%
k_{phred_w} (photo-demethylation water)	+50%	+0.02%	-0.73%	+0.02%	~ 0%	-0.09%	~ 0%
$K_{D_{Hg-silt}}$ (Hg-silt partition)	+50%	-11.1%	-6.4%	-20.1%	+1.1%	-6.6%	-37.8%
	-50%	+19.9%	+6.7%	+38.4%	-2.1%	+15.2%	+88.0%
$K_{D_{Hg-POM}}$ (Hg-POM partition)	+50%	+0.46%	0.43%	-3.2%	+0.1%	-1.0%	-7.4%
	-50%	-0.52%	-0.57%	+3.5%	-0.1%	+1.1%	+8.2%
$K_{D_{Hg-DOC}}$ (Hg-DOC partition)	+50%	+9.1%	+4.0%	+20.3%	-1.1%	+9.2%	+54.1%
	-50%	-11.8%	-7.6%	-26.1%	+1.3%	-9.9%	-57.9%
$K_{D_{MeHg-silt}}$ (MeHg-silt partition)	+50%	~ 0%	-7.9%	-0.01%	~ 0%	+1.36%	-~ 0%
	-50%	+0.01	+9.9%	+0.01%	~ 0%	-1.7%	-~ 0%
$K_{D_{MeHg-POM}}$ (MeHg-POM partition)	+50%	-0.01%	-8.6%	-0.01%	~ 0%	+1.32%	~ 0%
	-50%	+0.01%	+12.2%	+0.01%	~ 0%	-2.0%	~ 0%
$K_{D_{MeHg-DOC}}$ (MeHg-DOC partition)	+50%	+0.01%	+12.19%	+0.01%	~ 0%	-2.18%	~ 0%
	-50%	-0.01%	-16.8%	-0.02%	~ 0%	+2.8%	~ 0%

Table 16: Heatmap of variations in water and sediment concentrations of Hg species for each sensitivity simulation performed by varying boundary conditions (Table S13) and model parameters (Table S16) by ± 50%. A change in model output x is considered negligible ($\sim 0\%$) for $0.01 > x > -0.01$. Other thresholds are set for positive and negative variations in the range 0.01-1%, 1-5%, 5-10%, 10-25%, 25-50%, and >50%.

3 Supplementary Equations

$$ME = \frac{1}{N}\sum_{n=1}^{N} mod_i - obs_i \tag{107}$$

$$MAE = \frac{1}{N}\sum_{n=1}^{N} |mod_i - obs_i| \tag{108}$$

$$RMAE = \frac{\frac{1}{N}\sum_{n=1}^{N} |mod_i - obs_i|}{\frac{1}{N}\sum_{n=1}^{N} obs_i} \tag{109}$$

$$RMSE = \sqrt{\frac{1}{N}\sum_{n=1}^{N} (mod_i - obs_i)^2} \tag{110}$$

$$SI = \frac{RMSE}{\frac{1}{N}\sum_{n=1}^{N} obs_i} \tag{111}$$

4 Supplementary Figures

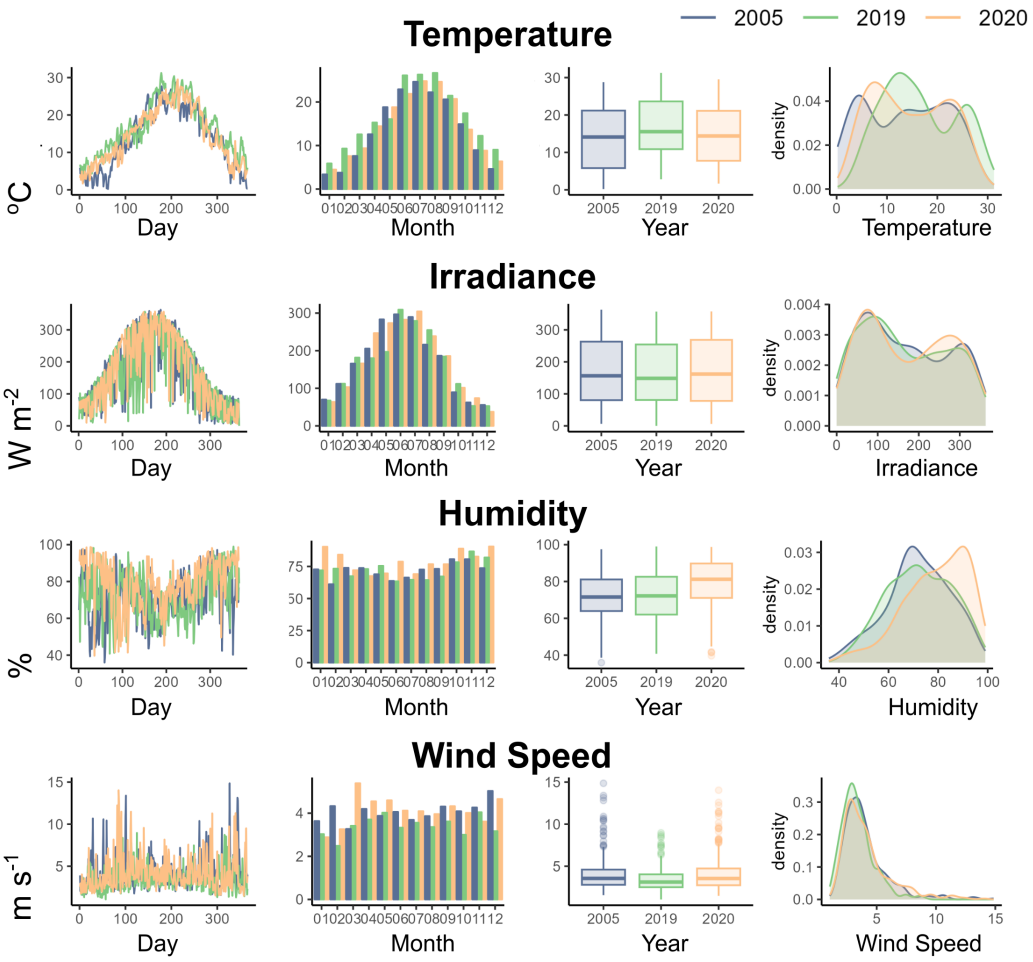

Figure 2: Meteorological model forcings for the three years simulated with the SHYFEM-Hg model. From left to right, the subplots show: the daily evolution of each forcing as provided as input to the model, barplots of the monthly means for the three years, boxplots of the annual distributions, and the probability distribution of the time-series.

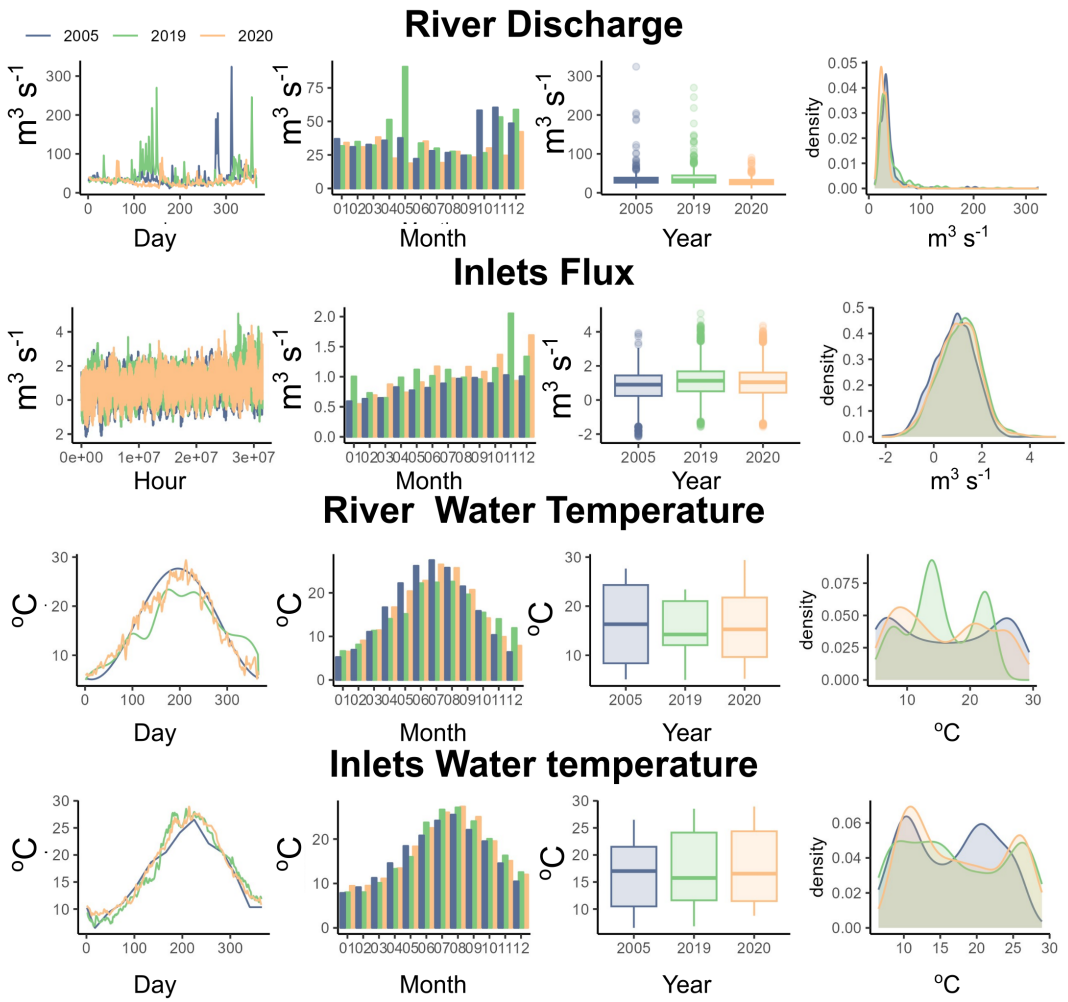

Figure 3: Hydrological data used to force the model for the three years simulated with the SHYFEM-Hg model. From left to right, the subplots show: the daily/hourly evolution of each forcing as provided as input to the model, barplots of the monthly means for the three years, boxplots of the annual distributions, and the statistical distribution of the data. River discharge and fluxes at inlets are calculated as the sum of all the contributions indicated in Supplementary Figure 4 and Figure 1b of the main text. Temperatures are for the Lido Inlet and the Dese River.

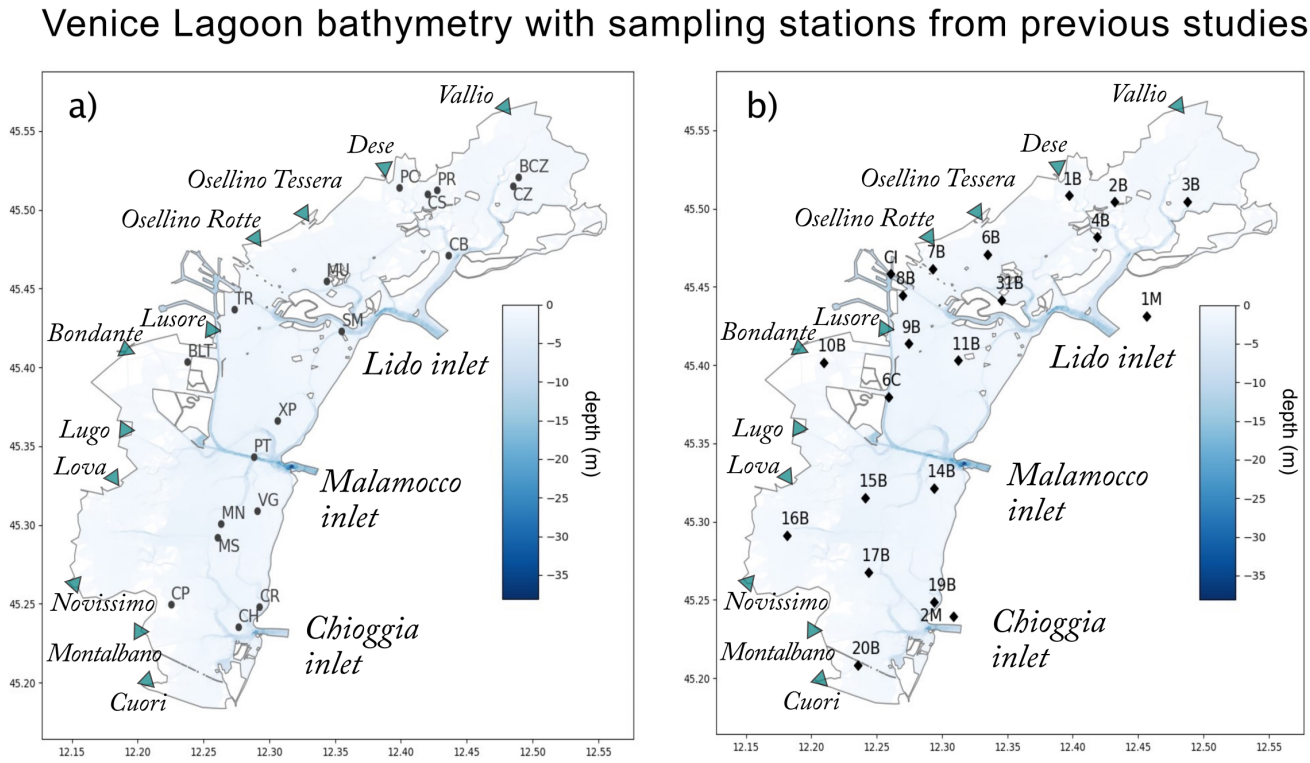

Figure 4: Bathymetry of the study area with the location of river mouths (triangles), lagoon inlets, and sampling stations for a) the Hg and MeHg data collected in 2001-2003 [33], and b) suspended particulate matter and particulate organic carbon in the water collected in 2005 [39].

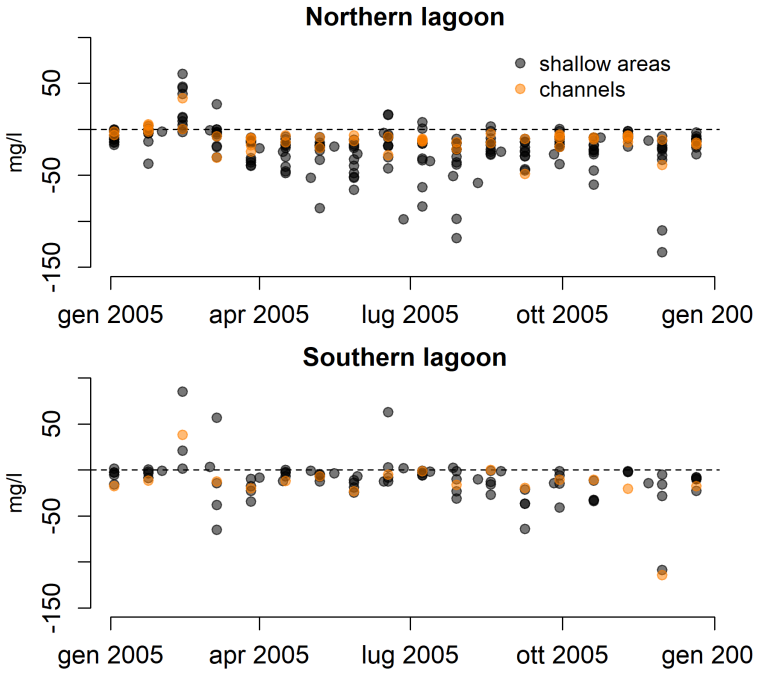

Figure 5: Model errors computed against observations of suspended particulate matter concentrations (see also Figure 4 in the main text) measured at the sampling stations shown in Figure S4b.

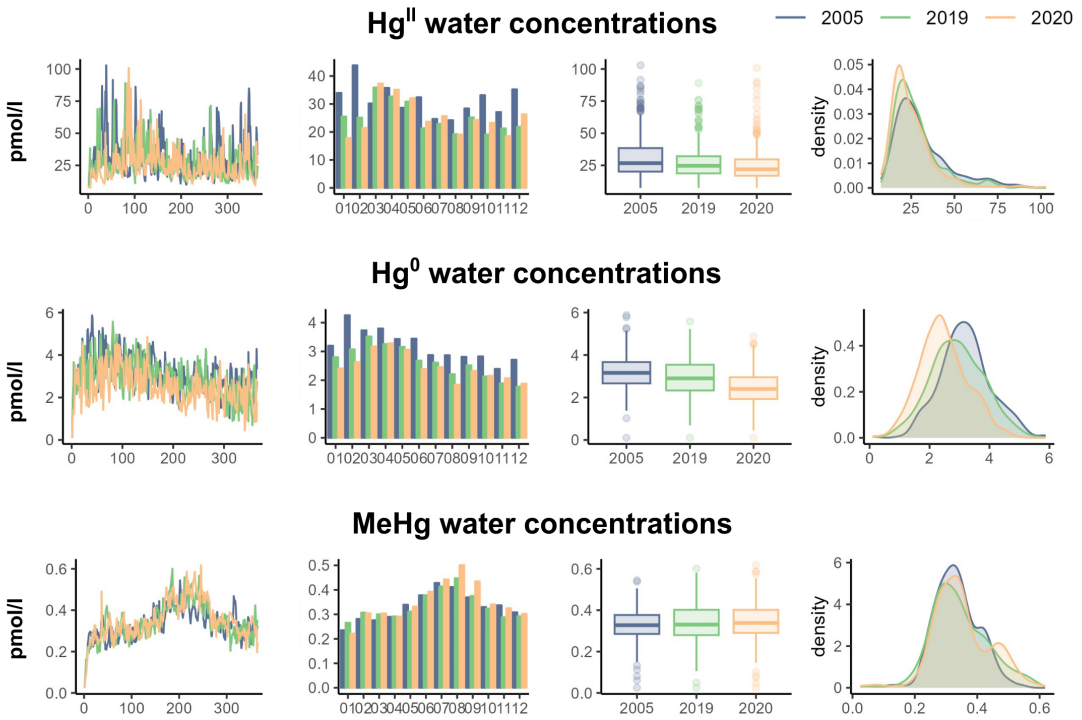

Figure 6: Model output of Hg species in water for the three years simulated. From left to right, the subplots show: the daily evolution of each state variable, barplots of the monthly means for the three years, boxplots of the annual distributions, and the probability distribution of the time-series

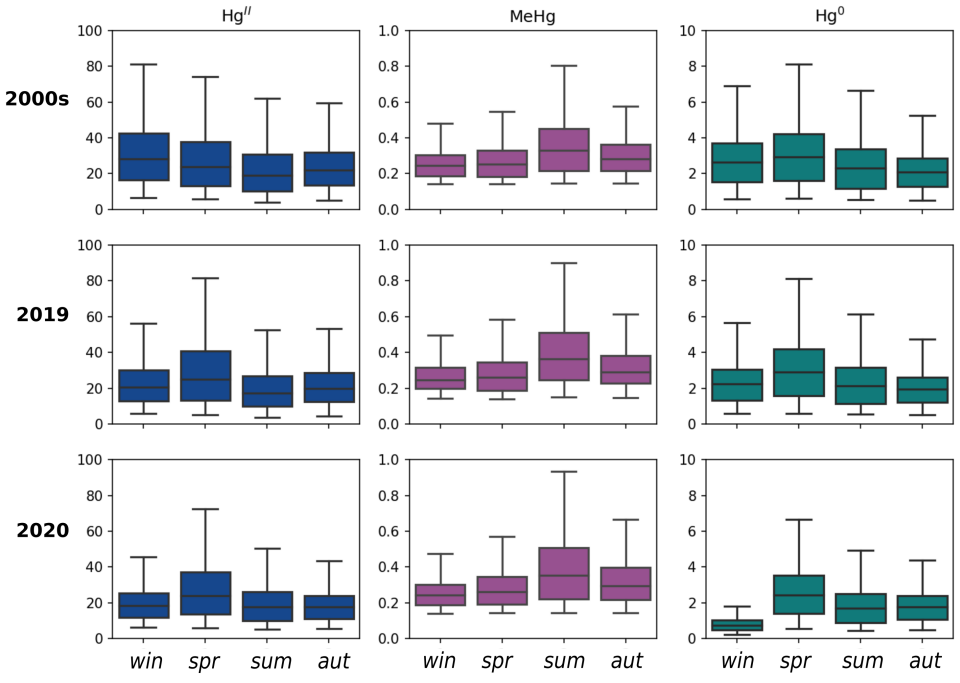

Figure 7: Boxplot showing the seasonal distribution of modeled Hg species in water for the three years simulated .

References

[1] Wool T.A. et al. *Water Quality Analysis Simulation Program (WASP) Version 6.0: User's Manual.* 2001.

[2] Rosati G., Solidoro C., and Canu D. "Mercury dynamics in a changing coastal area over industrial and postindustrial phases: Lessons from the Venice Lagoon". In: *Science of the Total Environment* 743.July (2020), pp. 1–15. ISSN: 18791026. DOI: 10.1016/j.scitotenv.2020.140586.

[3] Canu D. and Rosati G. "Long-term scenarios of mercury budgeting and exports for a Mediterranean hot spot (Marano-Grado Lagoon, Adriatic Sea)." In: *Estuarine, Coastal and Shelf Science* 198 (2017), pp. 518–528. ISSN: 02727714. DOI: 10.1016/j.ecss.2016.12.005.

[4] Melaku Canu D. et al. "A comprehensive assessment of the mercury budget in the Marano–Grado Lagoon (Adriatic Sea) using a combined observational modeling approach". In: *Marine Chemistry* 177 (2015), pp. 742–752. ISSN: 03044203. DOI: 10.1016/j.marchem.2015.10.013.

[5] Rosati G. et al. "Mercury in the Black Sea: new insights from measurements and numerical modeling". In: *Global Biogeochemical Cycles* 32.4 (2018), pp. 1–22. ISSN: 08866236. DOI: 10.1002/2017GB005700.

[6] Soerensen A.L. et al. "Eutrophication Increases Phytoplankton Methylmercury Concentrations in a Coastal Sea—A Baltic Sea Case Study". In: *Environmental Science & Technology* 50.21 (2016), pp. 11787–11796. DOI: 10.1021/acs.est.6b02717.

[7] Soerensen A.L. et al. "An improved global model for air-sea exchange of mercury: High concentrations over the North Atlantic". In: *Environmental Science & Technology* 44.22 (2010), pp. 8574–8580. ISSN: 0013936X. DOI: 10.1021/es102032g.

[8] Borges A. et al. "Variability of gas transfer velocity of CO2 in a macrotidal estuary (The Scheldt)". In: *Estuaries* 27 (Aug. 2004), pp. 593–603. DOI: 10.1007/BF02907647.

[9] Monperrus M. et al. "Mercury methylation, demethylation and reduction rates in coastal and marine surface waters of the Mediterranean Sea". In: *Marine Chemistry* 107 (1 2007), pp. 49–63. ISSN: 03044203. DOI: 10.1016/j.marchem.2007.01.018.

[10] Lehnherr I. et al. "Methylation of inorganic mercury in polar marine waters". In: *Nature Geoscience* 4 (April 2011), pp. 298–302. ISSN: 1752-0894. DOI: 10.1038/ngeo1134.

[11] Hines M. E. et al. "Mercury methylation and demethylation in Hg-contaminated lagoon sediments (Marano and Grado Lagoon, Italy)". In: *Estuarine, Coastal and Shelf Science* 113 (2012), pp. 85–89. DOI: 10.1016/j.ecss.2011.12.021.

[12] Marvin-DiPasquale M. et al. "Methyl-Mercury Degradation Pathways: A Comparison among Three Mercury-Impacted Ecosystems". In: *Environmental Science & Technology* 34 (23 2000), pp. 4908–4916. ISSN: 0013-936X. DOI: 10.1021/es0013125.

[13] Capo E. et al. "Anaerobic mercury methylators inhabit sinking particles of oxic water columns". In: *Water Research* 229 (Feb. 2023), p. 119368. ISSN: 00431354. DOI: 10.1016/j.watres.2022.119368.

[14] Ortiz V., Robert P. Mason, and J. Evan Ward. "An examination of the factors influencing mercury and methylmercury particulate distributions, methylation and demethylation rates in laboratory-generated marine snow". In: *Marine Chemistry* 177 (2015), pp. 753–762. ISSN: 03044203. DOI: 10.1016/j.marchem.2015.07.006.

[15] Barkay T., S.M. Miller, and A.O. Summers. "Bacterial mercury resistance from atoms to ecosystems". In: *FEMS Microbiology Reviews* 27.2-3 (2003), pp. 355–384. DOI: 10.1016/S0168-6445(03)00046-9.

[16] Rasmussen L.D. and Turner R. R. "Cell-Density-Dependent Sensitivity of a mer-lux Bioassay". In: 63 (8 1997), pp. 3291–3293.

[17] Cossart T. et al. "Role of phytoplankton in aquatic mercury speciation and transformations". In: *Environmental Chemistry* (2022). ISSN: 14482517. DOI: 10.1071/EN22045.

[18] Lamborg C. H. et al. "Dark Reduction Drives Evasion of Mercury From the Ocean". In: *Frontiers in Environmental Chemistry* 2 (Apr. 2021). DOI: 10.3389/fenvc.2021.659085.

[19] Lee C.S. and Fisher N.S. "Microbial generation of elemental mercury from dissolved methylmercury in seawater". In: *Limnology and Oceanography* 64.2 (2019), pp. 679–693. DOI: 10.1002/lno.11068.

[20] Poulain A.J. et al. "Biological and chemical redox transformations of mercury in fresh and salt waters of the high arctic during spring and summer". In: *Environmental Science & Technology* 41.6 (2007), pp. 1883–1888. ISSN: 0013936X. DOI: 10.1021/es061980b.

[21] Rothenberg S.E., Ambrose R.F, and Jay A.J. "Mercury cycling in surface water, pore water and sediments of Mugu Lagoon, CA, USA". In: *Environmental Pollution* 154.1 (2008), pp. 32–45. ISSN: 02697491. DOI: 10.1016/j.envpol.2007.12.013.

[22] Thomann R.V. and Di Toro. D.M. "Physico-chemical model of toxic substances in the Great Lakes". In: *Journal of Great Lakes Research* 9.(4) (1983), pp. 474–496.

[23] Stolpovsky K., Dale A.W., and Wallmann K. "A new look at the multi-G model for organic carbon degradation in surface marine sediments for coupled benthic-pelagic simulations of the global ocean". In: *Biogeosciences* 15.11 (2018), pp. 3391–3407. ISSN: 17264189. DOI: 10.5194/bg-15-3391-2018.

[24] Umgiesser G. et al. "A finite element model for the Venice Lagoon. Development, set up, calibration and validation". In: *Journal of Marine Systems* 51.1-4 SPEC. ISS. (2004), pp. 123–145. ISSN: 09247963. DOI: 10.1016/j.jmarsys.2004.05.009.

[25] Lick W. "Sediment Erosion". In: *Sediment and Contaminant Transport in Surface Waters*. 2008, pp. 45–97.

[26] DePinto J.V. et al. "Deposition and Resuspension of Particles and the Associated Chemical Transport across the Sediment–Water Interface". In: *Handbook of Chemical Mass Transport in the Environment*. Ed. by Louis J. Thibodeaux and Donald Mackay. Boca Raton: CRC Press, 2010. Chap. 10, pp. 253–299.

[27] Hwang K. and Mehta A.J. *Fine sediment erodibility in lake Okeechobee, Florida*. Tech. rep. 1989, p. 140.

[28] Avnimelech Y. et al. "Water content, organic carbon and dry bulk density in flooded sediments". In: *Aquacultural Engineering* 25.1 (Aug. 2001), pp. 25–33. ISSN: 0144-8609. DOI: 10.1016/S0144-8609(01)00068-1.

[29] Carniello L. et al. "Sediment dynamics in shallow tidal basins: In situ observations, satellite retrievals, and numerical modeling in the Venice Lagoon". In: *Journal of Geophysical Research: Earth Surface* 119 (4 2014), pp. 802–815. ISSN: 21699011. DOI: 10.1002/2013JF003015.

[30] Laurent O. Amoudry and Alejandro J. Souza. "Deterministic coastal morphological and sediment transport modeling: A review and discussion". In: *Reviews of Geophysics* 49 (2 June 2011). ISSN: 87551209. DOI: 10.1029/2010RG000341.

[31] Carniello L., a. Defina, and L. D'Alpaos. "Modeling sand-mud transport induced by tidal currents and wind waves in shallow microtidal basins: Application to the Venice Lagoon (Italy)". In: *Estuarine, Coastal and Shelf Science* 102-103 (2012), pp. 105–115. ISSN: 02727714. DOI: 10.1016/j.ecss.2012.03.016.

[32] Han S. et al. "Biogeochemical factors affecting mercury methylation in sediments of the Venice Lagoon, Italy." In: *Environmental toxicology and chemistry / SETAC* 26 (4 2007), pp. 655–63. ISSN: 0730-7268. DOI: 10.1897/06-392R.1. URL: http://www.ncbi.nlm.nih.gov/pubmed/17447549.

[33] Bloom N.S. et al. "Seasonal cycling of mercury and monomethyl mercury in the Venice Lagoon (Italy)". In: *Marine Chemistry* 91.1-4 (2004), pp. 85–99. DOI: 10.1016/j.marchem.2004.06.002.

[34] Sharif A. et al. "Fate of mercury species in the coastal plume of the Adour River estuary (Bay of Biscay, SW France)". In: *Science of The Total Environment* 496 (2014), pp. 701–713. ISSN: 0048-9697. DOI: https://doi.org/10.1016/j.scitotenv.2014.06.116. URL: https://www.sciencedirect.com/science/article/pii/S0048969714009899.

[35] Schaefer J. K. et al. "Role of the bacterial organomercury lyase (MerB) in controlling methylmercury accumulation in mercury-contaminated natural waters". In: *Environmental Science and Technology* 38 (16 2004), pp. 4304–4311. ISSN: 0013936X. DOI: 10.1021/es049895w.

[36] Amos C. L. et al. "The erosion rates of cohesive sediments in Venice lagoon, Italy". In: *Continental Shelf Research* 30 (8 2010), pp. 859–870. ISSN: 02784343. DOI: 10.1016/j.csr.2009.12.001.

[37] Jože Kotnik et al. "Mercury speciation in the Adriatic Sea". In: *Marine Pollution Bulletin* 96 (1-2 2015), pp. 136–148. DOI: 10.1016/j.marpolbul.2015.05.037. URL: http://linkinghub.elsevier.com/retrieve/pii/S0025326X15002945.

[38] Rossini P. et al. "Atmospheric bulk deposition to the lagoon of Venice: Part I. Fluxes of metals, nutrients and organic contaminants". In: *Environment International* 31 (7 SPEC. ISS. 2005), pp. 959–974. ISSN: 18736750. DOI: 10.1016/j.envint.2005.05.006.

[39] MAV-CVN. *Attività di monitoraggio ambientale della laguna di Venezia. Esecutivo del II stralcio triennale (2002 - 2005) - Environmental monitoring in the Venice Lagoon. Triennial Report (2002 - 2005) (in italian)*. Tech. rep. 2005, p. 91.